Computation of Nonequilibrium, Supersonic Three-Dimensional Inviscid Flow over Blunt-Nosed Bodies

John V. Rakich,* Harry E. Bailey,† and Chul Park‡
NASA Ames Research Center, Moffett Field, California

A computer code based on the method of characteristics is applied to the study of two- and three-dimensional chemical nonequilibrium flow over sharp- and blunt-nosed bodies. Nonequilibrium flow over a wedge is used to show the approach to equilibrium flow and to demonstrate the nature of the reaction zone behind the bow shock wave. The structure and development of a blunt-body entropy layer in nonequilibrium flow is examined for a blunt cone at zero incidence. Three dimensional computations for the Space Shuttle body at 30 deg angle of attack are presented. A nondimensional scaling parameter, the Damköhler number (the ratio of flow time to chemical reaction time) is calculated and its significance discussed.

Nomenclature

a = frozen speed of sound, Eq. (8)
H = total enthalpy
h = enthalpy
h_m^0 = formation energy of mth species
K_n = equilibrium constant of nth reaction
k_{nm} = reverse reaction rate coefficient for nth reaction with mth species as the third body
M = Mach number
$\bar{m}$ = average molecular weight (28.8 for air)
N_x, N_r, N_ϕ = components of body surface normal vector
p = pressure
q_m = concentration of mth species, g-mole·g^{-1}
s = streamline direction
s,n,t = orthogonal unit vectors
T = temperature
t = time
u,v,w = velocity components along x, r, and Φ
V = total velocity ($V = V_s$)
x,r,Φ = cylindrical coordinates
Z = compressibility
α = angle of attack
β = $(M^2-1)^{1/2}$
γ = specific heat ratio
δ = shock angle in cross plane
ξ,η,ζ = nonorthogonal shock-layer coordinates
$\bar{\eta}$ = nondimensional distance from body, $\bar{\eta} = (r-r_B)/(r_s-r_B)$
θ = flow angle from x axis in meridional plane, $\tan^{-1} v/u$
κ_n = overall reverse reaction rate coefficient for nth reaction
μ = Mach angle, $\sin^{-1}(1/M)$
ρ = density
σ = shock angle in meridional plane
Φ = azimuthal angle, cylindrical coordinates
ϕ = crossflow angle, $\sin^{-1}(w/V)$
χ_m = mole fraction of species m, $\chi_m = \bar{m} q_m$
ψ = chemical source term, Eq. (9)
ω_m = chemical production rate of mth species, g-mole·g^{-1}·s^{-1}

Subscripts

B = body
i,j,τ = indices for radial position of mesh points
m = index denoting chemical species
n = index denoting chemical reaction
N = shock-normal component
S = shock
∞ = freestream condition

Superscripts

N = total number of species

Introduction

A RENEWED interest in flows with finite-rate chemical reactions, that is, nonequilibrium flows, has been generated by the recent flight of the Space Shuttle. Because of the high-altitude entry trajectory of the Shuttle a considerable period of nonequilibrium flow occurs during atmospheric entry. Flight data[1] show significant noncatalytic surface effects which reduce the surface temperature. Because of the size of the vehicle, the flow cannot be simulated by current ground-based facilities. Therefore, there is a need to calculate the dissociated gas environment around this blunt-nosed vehicle flying at large angle of attack. For previous manned atmospheric entry-vehicles, nonequilibrium effects could be determined by a boundary-layer analysis alone, using equilibrium properties for the inviscid external flow. For the Shuttle, however, a large part of the inviscid flow is out of equilibrium. Therefore, a fully reacting inviscid solution is needed to provide the necessary boundary conditions for a solution of the reacting viscous boundary layer. With this application in mind, the present paper describes the general gasdynamic features of nonequilibrium flows and discusses the feasibility of their numerical prediction.

One-dimensional nonequilibrium flows received considerable attention in the 1960s. During that period the computational problems associated with the stiffness of the chemical rate equations were identified and solutions developed (see, e.g., Refs. 2-4). Some two-dimensional calculations were done at that time[4-10] but neither the computer technology nor the computational methods were as yet adequate for three-dimensional flows. Three-dimensional flow calculations were accomplished for nozzles by Taylor and Hoffman[11] and for blunt-body flows by Li.[12] In 1973, Rakich and Park[13] presented computations for three-dimensional nonequilibrium flows around pointed bodies. The nonequilibrium flow over a blunt nose has been reexamined by Bailey and Rizzi[14] who used a "finite volume" technique.

The present paper presents some results and problems that have arisen in calculating nonequilibrium flows over blunt-nosed bodies. As is well known, blunt-body flows develop a thin "entropy layer" near the body surface, in which strong gradients of flow properties occur. This entropy layer occurs

Presented as Paper 75-835 at the AIAA 8th Fluid and Plasma Dynamics Conference, Hartford, Conn., June 16-18, 1975; submitted Jan. 26, 1982; revision received Sept. 7, 1982.

*Research Scientist. Associate Fellow AIAA.
†Research Scientist.
‡Research Scientist. Member AIAA.

also in reacting flows but is more complex because of the chemical species gradients. Even a pointed cone at zero incidence develops a weak entropy layer in nonequilibrium flow. In addition, a thin layer with strong gradients, due entirely to chemical reactions, forms near the bow shock wave.[13] This layer may be called a "chemical reaction front" because a small pressure rise occurs across the layer and the layer becomes infinitely thin in the equilibrium limit.

In this paper, the effects of chemical reactions on the entropy layer are evaluated by comparing the flow over pointed and blunted cones. Sample flight predictions are presented for the blunt-nosed Shuttle body at a 30 deg angle of attack.

Analysis

Gasdynamic Equations

The conservation equations governing the flow of nonviscous, nonheat-conducting but reacting gas are[5,15]

Mass

$$D\rho/Dt+\rho \operatorname{div} V=0 \tag{1}$$

Momentum

$$\rho(DV/Dt)+\operatorname{grad} p=0 \tag{2}$$

Energy

$$\rho(Dh/Dt)-Dp/Dt=0 \tag{3}$$

Species

$$Dq_m/Dt=\omega_m \quad (m=1,2,\ldots,N) \tag{4}$$

These equations are supplemented by the equation of state in the form

$$h=h(p,\rho,q_m) \tag{5}$$

The operator D/Dt denotes the Eulerian derivative following a fixed mass of fluid

$$D/Dt=\partial/\partial t+V\cdot\operatorname{grad} \tag{6}$$

In order to obtain the compatibility equations of the theory of characteristics, one must obtain a differential relation between pressure and density. This is accomplished by differentiating the equation of state [Eq. (5)] and using Eq. (3) to obtain

$$D\rho/Dt=1/a^2\,(Dp/Dt)-\psi \tag{7}$$

where a^2 is the frozen speed of sound[15]

$$a^2\equiv\left(\frac{\partial h}{\partial \rho}\right)_{p,q_m}\Big/\left[\frac{1}{\rho}-\left(\frac{\partial h}{\partial p}\right)_{\rho,q_m}\right] \tag{8}$$

and where

$$\psi=\sum_{m=1}^{N}\omega_m\left(\frac{\partial h}{\partial q_m}\right)_{p,\rho}\Big/\left(\frac{\partial h}{\partial \rho}\right)_{p,q_m} \tag{9}$$

The subscripts on the partial derivatives in Eqs. (8) and (9) denote the variables held constant. The term ψ in Eq. (7) behaves like a source or sink of mass and is therefore called the nonequilibrium source term; it depends on the rates of production ω_m of chemical species and tends to zero for a frozen gas, thus reducing Eq. (7) to the familiar perfect-gas relation. It will be seen in a later section that this source term has a strong influence on the approach to equilibrium flow.

Equation (7) can be combined with Eqs. (1) and (2) to obtain the equations of steady gas dynamics. These are given here in their intrinsic form

Mass and s momentum

$$(\beta^2/\rho V^2)\,s\cdot\operatorname{grad} p+\operatorname{div} s-(\psi/\rho V)=0 \tag{10}$$

Mass and n momentum

$$(1/\rho V^2)\,n\cdot\operatorname{grad} p+t\cdot\operatorname{curl} s=0 \tag{11}$$

Mass and t momentum

$$(1/\rho V^2)\,t\cdot\operatorname{grad} p-n\cdot\operatorname{curl} s=0 \tag{12}$$

where s, n, and t are a triad of orthogonal unit vectors, $s=V/V$ being aligned with the streamlines, and $\beta^2=M^2-1$. We note that the present equations with reactions differ from the perfect-gas equations only by the additional source term $\psi/\rho V$ in Eq. (10) and by the use of the frozen speed of sound [Eq. (8)].

The compatibility equations of the theory of characteristics follow directly from Eqs. (10-12) by procedures described in numerous texts (see Refs. 16 and 17 for the methods used in the present paper). The form of the equations is unaffected by the presence of chemical reactions and the only additional term involves the source term ψ.

Temperature Equation

Since the temperature and species concentrations are strongly coupled, it is advantageous to account for the variation of temperature between points on the finite-difference grid. The temperature variation is obtained by expressing the enthalpy as a function of temperature

$$h=h(p,T,q_m) \tag{13}$$

Differentiating Eq. (13) and using the energy equation, Eq. (3), one obtains

$$\frac{DT}{Dt}=\left(\frac{\partial h}{\partial T}\right)_{p,q_m}^{-1}\left\{\left[\frac{1}{\rho}-\left(\frac{\partial h}{\partial p}\right)_{T,q_m}\right]\frac{Dp}{Dt}-\sum_{m=1}^{N}\left(\frac{\partial h}{\partial q_m}\right)_{p,T}\frac{Dq_m}{Dt}\right\} \tag{14}$$

Equation (14) with the operator of Eq. (6) gives the variation of temperature in the direction s. The system is completed by the integrated form of the energy equation

$$H=h+(V^2/2)=\text{const} \tag{15}$$

The solution of these equations is described below in the section on finite-difference methods. The particular form of the state and rate equations for the present gas model is considered next.

Reacting Gas Model

Air is considered to be a mixture of 21% oxygen and 79% nitrogen. In the supersonic flow region presently under consideration for Space Shuttle applications, the gas temperature varies typically between 2000 and 5000 K and seldom exceeds 6000 K. In this temperature range, negligible ionization occurs. The small number of ions, mostly NO^+, that may be present in the flow do not significantly participate in the molecular dissociation reations as a catalyst. Hence ionized species are excluded from the calculations. The five species considered in the calculations, atomic oxygen (O), atomic nitrogen (N), nitric oxide (NO), molecular oxygen (O_2), and molecular nitrogen (N_2), are indexed $m=1$-5, respectively. The concentrations $q_m, m=1$-5 are expressed in the units of g-mole$\cdot$g^{-1}. The vibrational excitation of nitric

oxide, oxygen, and nitrogen molecules is approximated by the "half-excited" model of Lighthill.[18] That is, rather than introducing nonequilibrium vibrational excitation, the vibrational mode is assumed to be excited always to such an extent that its energy content is $RT/2$, where R is the gas constant; $RT/2$ is half of the fully excited equilibrium value attained at high temperatures. The Lighthill model is considered appropriate for the present applications primarily because the vibrational energy is a small fraction of the static enthalpy and hence does not influence the flow properties greatly. Figure 1 compares the enthalpy contents in the vibrational modes between the present model and the rigorous air model of Hilsenrath and Klein[19] under equilibrim conditions in the range of temperatures where the vibrational excitation is significant. As seen in Fig. 1, there is only a small difference between the energy content of the two models.

The reactions that were considered in the present calculation are shown in Table 1; the equilibrium constants for the reactions are also shown. The equilibrium constants K_n are taken from Logan and Treanor[20] and are approximated by the product of a second-order polynomial and an exponential factor as shown in the table. The reaction rates ω_m in units of g-mole·g^{-1}·s^{-1} are tabulated in Table 2. As shown in Table 2, the rates are expressed terms of reverse reaction rates κ instead of the corresponding forward rates, as is more common.[15] This approach avoids an exponential overflow in the computation; if the forward rates are used, a multiplication of the form $\exp(113{,}000/T)\times\exp(-113{,}000/T)$ must be carried out, an operation that causes the numerical computations to fail at low temperatures. By adopting the reverse rates, this difficulty disappears. The rate expressions are given only for $m=1$, 2, and 3, since q_4 and q_5 are related to q_1, q_2, and q_3 via the mass conservation law that dictates

$$q_4 = 0.21/\bar{m} - \tfrac{1}{2}(q_1+q_3) \tag{16}$$

$$q_5 = 0.79/\bar{m} - \tfrac{1}{2}(q_2+q_3) \tag{17}$$

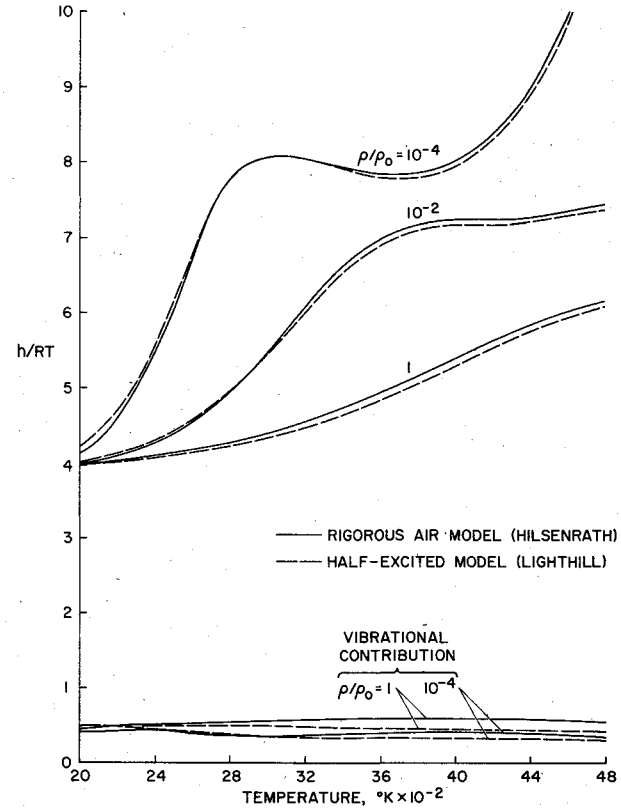

Fig. 1 Comparison of energies at equilibrium between rigorous and half-excited vibration model for air.

The necessary reverse rate constants are taken from Vincenti and Kruger[15] and are summarized in Tables 3 and 4.

With the present assumptions, the state equations can be written

$$p=\rho RTZ \tag{18}$$

$$h=(p/\rho)(3+Z)/Z+h_1^0q_1+h_2^0q_2+h_3^0q_3 \tag{19}$$

where the compressibility Z is

$$Z=1+(q_1+q_2)\bar{m}/2 \tag{20}$$

Here $\bar{m}$ is the average molecular weight of air that, according to the present model, is 28.8 g/mole. The net formation energies h_1^0, h_2^0, and h_3^0 have the values given in Table 5.

Finite Difference Methods

The finite-difference computations advance the solution from an initial data surface, stepping forward in the reference planes $\Phi=$const. At a typical point (i,j), the compatibility equations are solved by a standard explicit predictor-corrector method.[16,17] After each predictor or corrector step, the species conservation equations are solved by an implicit method using the pressure and velocity from the previous predictor or corrector. The density and species concentrations are obtained from the state and rate equations and the entire process is repeated. One corrector is sufficient for second-order accuracy but two correctors are usually employed. The reader can get additional details on the explicit methods from the cited references. Some explanation is needed, however, of the methods used for the rate equations.

Implicit Integration of the Species Equations

Only $(N-2)$ of the N species conservation equations need to be integrated, because the mass conservation Eqs. (16) and (17) eliminate two variables. However, in the present approach the temperature is determined from Eq. (14) simultaneously with the species concentrations because of the strong nonlinear dependence of species on temperature. For the present gas model the following four equations are solved

$$\frac{\partial q_m}{\partial s}=\frac{\omega_m}{V} \quad (m=1,2,3) \tag{21}$$

and

$$\frac{\partial T}{\partial s}=\frac{1}{(3+Z)R}\left[\frac{1}{\rho}\frac{\partial p}{\partial s}-\left(\frac{\bar{m}}{2}+h_1^0\right)\frac{\partial q_1}{\partial s}-\left(\frac{\bar{m}}{2}+h_2^0\right)\frac{\partial q_2}{\partial s}-h_3^0\frac{\partial q_3}{\partial s}\right] \tag{22}$$

The first term in the brackets of Eq. (22) represents the heating or cooling by isentropic compression or expansion. The rest of the terms denote the conversion of heat into chemical energy. The pressure variation, $\partial p/\partial s$, is known as a result of integration of the compatibility equations along the characteristics and is taken to be constant along the streamline, that is, a linear variation in pressure is assumed along the streamline. The four equations, three from Eq. (21) plus Eq. (22), are then integrated along the streamline using an implicit integration scheme[3] to insure numerical stability. This scheme requires numerical evaluation of the matrix $(\partial\omega_m/\partial q_n)$ at each point, but the eigenvalues of the matrix need not be calculated.

Shock Boundary Conditions

At the shock surface, the chemical species concentrations are held constant, that is, reactions are frozen. As a con-

Table 1 Reactions considered and their equilibrium constants

n	Reaction	Equilbrium constant K_n [a]
1	$O_2 + X \rightleftharpoons O + O + X$	$K_1 \equiv (q_1^2/q_4)_e = (28.736 - 2.624\times10^{-3}T + 9.894\times10^{-8}T^2)\exp(-59{,}500T^{-1})$
2	$N_2 + X \rightleftharpoons N + N + X$	$K_2 \equiv (q_2^2/q_5)_e = (21.324 - 1.23\times10^{-3}T + 1.1091\times10^{-7}T^2)\exp(-113{,}000T^{-1})$
3	$NO + X \rightleftharpoons N + O + X$	$K_3 \equiv (q_1q_2/q_3)_e = (6.1007 - 5.105\times10^{-4}T + 2.957\times10^{-8}T^2)\exp(-75{,}500T^{-1})$
4	$NO + O \rightleftharpoons O_2 + N$	$K_4 \equiv (q_4q_2/q_3q_1)_e = K_3/K_1$
5	$N_2 + O \rightleftharpoons NO + N$	$K_5 \equiv (q_2q_3/q_1q_5)_e = K_2/K_3$
6	$N_2 + O_2 \rightleftharpoons NO + NO$	$K_6 \equiv (q_3^2/q_4q_5)_e = (K_1K_2/K_3^2)\exp(-21{,}500T^{-1})$

[a] Subscript e designates equilibrium condition; temperature T is in K.

Table 2 Species production rates[a]

n	ω_n
1	$(\partial q_1/\partial t)_1 + (\partial q_1/\partial t)_3 + (\partial q_1/\partial t)_4 - (\partial q_1/\partial t)_5$
2	$(\partial q_2/\partial t)_2 + (\partial q_1/\partial t)_3 - (\partial q_1/\partial t)_4 + (\partial q_1/\partial t)_5$
3	$-(\partial q_1/\partial t)_3 + (\partial q_1/\partial t)_4 + (\partial q_1/\partial t)_5 + (\partial q_3/\partial t)_6$

Definition of terms

$(\partial q_1/\partial t)_1 \equiv 2\kappa_1\rho(K_1q_4 - \rho q_1^2)$

$(\partial q_1/\partial t)_3 \equiv \kappa_3\rho(K_3q_3 - \rho q_1q_2)$

$(\partial q_1/\partial t)_4 \equiv -\kappa_4\rho(K_4q_1q_3 - q_2q_4)$

$(\partial q_1/\partial t)_5 \equiv \kappa_5\rho(K_5q_1q_5 - q_2q_3)$

$(\partial q_2/\partial t)_2 \equiv 2\kappa_2\rho(K_2q_5 - \rho q_2^2)$

$(\partial q_3/\partial t)_6 \equiv 2\kappa_6\rho(K_6q_4q_5 - q_3^2)$

[a] Density ρ in g/cm^3.

Table 3 Reverse rate coefficients k_{nm} for three-body reactions

$$\kappa_n = \sum_{m=1}^{5} k_{nm}q_m, \quad n = 1,3$$

n	m	k_{nm}
1	1	$4.14\times10^{18}T^{-1}\exp(-171.5T^{-1})$
1	2	k_{11}
1	3	$k_{11}/3$
1	4	$k_{11}/3$
1	5	$k_{11}/3$
2	1	$9.0\times10^{14}\exp(500T^{-1})$
2	2	k_{21}
2	3	$k_{21}/3$
2	4	$k_{21}/3$
2	5	$k_{21}/3$
3	1	$1.28\times10^{17}T^{-0.5}$
3	2	k_{31}
3	3	$k_{31}/2$
3	4	$k_{31}/2$
3	5	$k_{31}/2$

Here $n = 1,2,3$ refer to reactions indicated in Table 1, and $m = 1$-5 indicate species acting as the third body of reaction. Temperature T is in K.

Table 4 Reverse rate coefficients κ_n for binary reactions $n = 4,5,6$

n	κ_n
4	$1.015\times10^{10}T\exp(-3096T^{-1})$
5	1.6×10^{13}
6	0.0

Temperature T in K.

Table 5 Formation energies

m	Species	h_m^0, J/K$_g$
1	O	2.451×10^{11}
2	N	4.706×10^{11}
3	NO	0.9128×10^{11}

sequence of the frozen reactions, the shock conditions are similar to those for perfect-gas flow. However, because of the present gas model, the shock jump conditions are slightly different from the usual. Since the molecular vibrations are assumed to be half excited behind the bow shock and not excited in front of the shock, the ratio of specific heats γ changes across the shock. In front of the shock $\gamma_1 = 7/5$ and behind the shock $\gamma_2 = 4/3$. Under this assumption the shock pressure ratio is

$$\frac{p_2}{p_1} = \left(\frac{1}{1+\gamma_2}\right)(1+\gamma_1M_{1N}^2) + \sqrt{\gamma_2^2 + \gamma_1M_{1N}^2\left[\gamma_1M_{1N}^2 - 2\left(\frac{\gamma_2^2-\gamma_1}{\gamma_1-1}\right)\right]} \tag{23}$$

Stability

The implicit scheme used for the rate equations is expected to be unconditionally stable, and this is confirmed by tests. The overall calculation, including the explicit calculation of the compatibility equations, should therefore be controlled by the Courant-Friedrichs-Lewey (CFL) condition. Lomax and Bailey[3] recommend that all of the equations be differenced by the same (implicit) method. If this procedure is followed, stability is insured by a theoretical analysis of a linear system.[3] Nevertheless, experience with the present mixed-difference scheme applied to this nonlinear problem indicates that the system has the same stability constraints as the nonreacting case.

Results

It will be helpful, before presenting the detailed computational results, to describe in a qualitative manner the nonequilibrium flow over pointed and blunted cones at zero incidence. Figure 2 shows the shock shape and distribution of a typical species, say atomic oxygen, for a pointed cone. Even though the body is conical, the flow has a scale that depends on the time constant for pertinent species reactions. Near the

apex of a cone, one can find a region where there is not sufficient time for reactions to occur. Here the flow is conical, and the species concentrations are practically equal to the freestream values in front of the shock (frozen flow). The shock angle is equal to that for a perfect-gas flow with a constant ratio of specific heats.§ Thus, if the freestream is undissociated, the terms frozen and perfect gas mean the same thing. As the fluid moves away from the apex and the species begin to equilibrate to the local temperature, the flow enters the nonequilibrium region. Far downstream from the apex where the physical dimensions are large, all of the reactions can go to completion in a short distance relative to the shock standoff distance; this is called the equilibrium region. In the equilibrium approximation it is assumed that the chemical species instantaneously adjust to the local pressure and temperature. Computations of this type are easily performed with equilibrium equations of state. However, taking nonequilibrium flows to the equilibrium limit is not as easy because of the steep gradients at the shock. Note also that a weak entropy layer forms near the body because the streamline at the apex passes through a stronger shock than the outboard streamlines. In the equilibrium approximation the structure at the shock and near the body is neglected.

Damköhler's Number

Damköhler's first number is a nondimensional parameter that is helpful in determining the degree of importance of finite-rate chemical reactions. In general terms the number is defined as

$$Da \sim \frac{\text{flow time}}{\text{chemical relaxation time}} \tag{24}$$

For small Da the flow is frozen, and for large Da the flow tends to equilibrium. A problem occurs in practice, however, because there usually is more than one relaxation time; no clear precedent seems to exist in the fluid dynamics literature. Therefore it is here proposed to form a chemical relaxation time from the source term ψ defined in Eq. (9). This is the natural choice to make on inspection of the streamwise momentum equation [Eq. (10)]. Accordingly, a Damköhler number may be written as

$$Da_s = \psi_s x/\rho_s V_s \tag{25}$$

where ψ_s, ρ_s, and V_s are evaluated at conditions behind the bow shock wave and x is the coordinate distance to the point on the shock. The source term ψ makes sense only if evaluated at an elevated temperature somewhere behind the bow shock wave, that is, the freestream value would not be meaningful. Specific values of Da_s will be presented and discussed in the next section.

Another Damköhler number, which is important to the properties of the numerical calculation, is that based on the mesh size. Thus, a "mesh Damköhler number" is defined by

$$Da_\Delta = \psi\Delta/\rho V \tag{26}$$

where Δ is a significant mesh dimension, here taken as $\Delta\eta$.

Two-Dimensional Flow and the Chemical Reaction Front

To illustrate some basic features of nonequilibrium flows, and some problems arising in the numerical solution, we next show results for flow over a wedge. Figure 3 shows the variation of shock angle with distance, and Fig. 4 presents the distribution of atomic oxygen, pressure, flow angle, and the

§Note that a two-γ jump condition [Eq. (23)] should properly be used for the present gas model. This was done for most of the results shown, but a single γ was used for the Shuttle case presented in order to match the blunt-body starting solution.

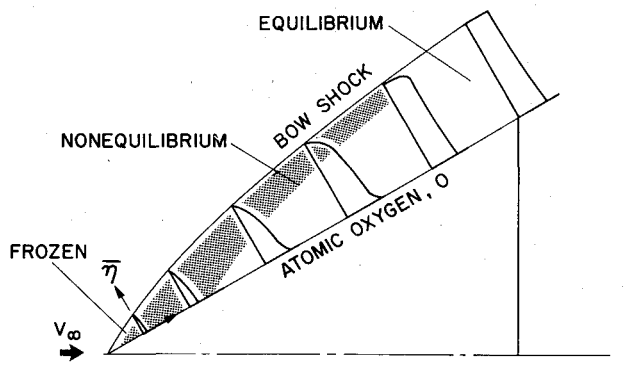

Fig. 2 Schematic profiles of atomic oxygen between body and shock of a pointed cone.

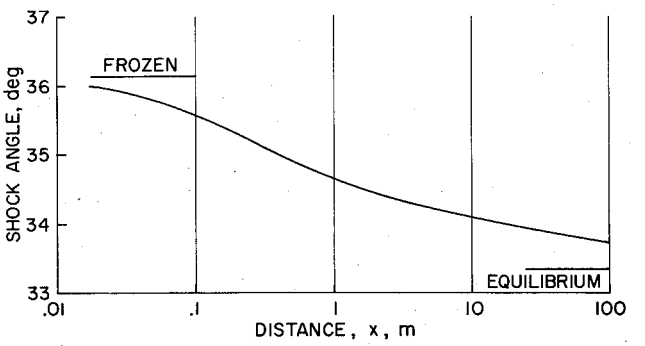

Fig. 3 Shock angle for nonequilibrium flow over a 30 deg wedge.

chemical source term ψ between the body and shock surfaces. The distributions are shown at various distances from the apex, from frozen to near-equilibrium conditions. The wedge has a 30 deg half-angle and the freestream conditions are those at an altitude of 65.5 km and flight velocity of 6.7 km/s. These conditions are typical of the high laminar heating portion of the Shuttle entry trajectory. The specific conditions used are given in Table 6 and will be used for all the results in this paper.

The wedge results in Fig. 4 show that a region of steep gradients forms near the bow shock wave. These gradients in the η direction steepen as x increases, tending to a discontinuity in the equilibrium flow limit. The reason for the developing discontinuity is that the flow first passes through the usual gasdynamic shock with frozen chemical reactions, and then undergoes an additional compression and entropy rise that is entirely due to the chemical reactions. This pressure rise is here termed a chemical reaction front because it tends to a discontinuity in the equilibrium limit. In this limiting case, the sum of property changes across the gasdynamic and chemical reaction fronts results in the usual equilibrium property changes.

The chemical reaction front is best explained with the flow angles shown in Fig. 4c. Both equilibrium and frozen flows result in a uniform flow angle ($\theta = 30$ deg) everywhere behind the bow shock. However, the shock angle is different in the two limiting flows (see Fig. 3). When a nonequilibrium shock is taken to the equilibrium limit, the equilibrium shock angle must result. Therefore, the nonequilibrium flow angle will be less than the equilibrium value, being the result of the frozen jump condition evaluated at the equilibrium shock angle. The nonequilibrium flow angle is just under 28 deg in Fig. 4c, and the nonequilibrium solution tends to that value with increasing x. In the limit $x \to \infty$, the flow angle must change from less than 28 to 30 deg in an infinitesimal distance. The discontinuous change is small but real.

This tendency for near-equilibrium flow to become discontinuous near the shock wave can cause serious numerical problems. When calculating near-equilibrium flow

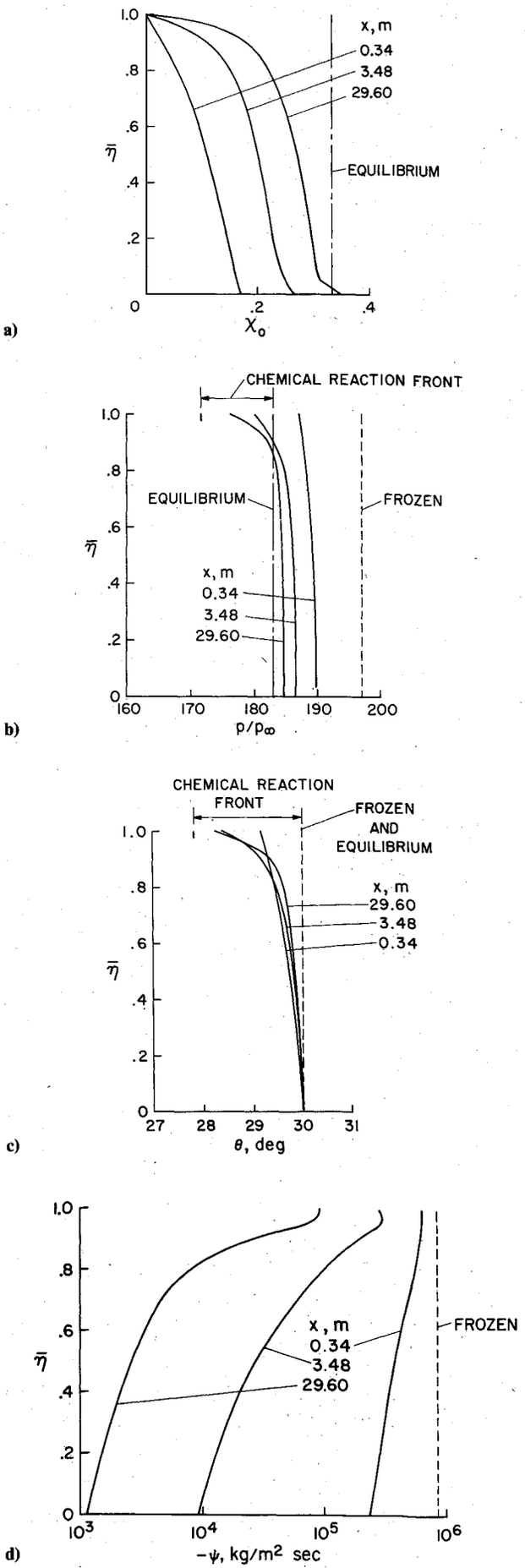

Fig. 4 Shock layer properties for nonequilibrium flow over a 30 deg wedge, $V_\infty = 6.7$ km/s, altitude = 65.5 km: a) atomic oxygen mole fraction χ_O; b) pressure; c) flow angle; d) nonequilibrium source term.

Table 6 Freestream conditions for computations

Velocity	6.7 km/s	(22,000 ft/s)
Altitude	65.5 km	(215,000 ft)
Pressure	10.85 N/m^2	(0.2218 lb/ft^2)
Density	1.156×10^{-4} kg/m^3	(3.028×10^{-7} slug/ft^3)
Temperature	237.1 K	(426.7 °R)
Sound speed		
$\gamma = 7/5$	0.3083 km/s	(1012.5 ft/s)
$\gamma = 4/3$	0.3010 km/s	(988.1 ft/s)

with the present computer code, it was found that the calculation for the shock angle failed to converge, resulting in a complete loss of accuracy. Of course, the accuracy could be improved by refining the mesh; however, this is often impractical and it delays the problem for only some small distance. Extensive studies were therefore made in an effort to find a procedure that would permit an accurate approach to equilibrium flow. A completely satisfactory solution has not yet been found, although some improvement was achieved after observing that the source term ψ [Eq. (9)] had a strong effect on the shock solution. To be more precise, the shock angle is found by matching the pressure from the Hugoniot shock jump conditions with the pressure behind the shock. From Fig. 4d, it is evident that ψ may change by an order of magnitude over a mesh interval near the shock. In the standard method, the average value of ψ is taken between the shock and the first field point. The present method is to evaluate ψ, using the temperature at the first field point in from the shock, and the freestream species.

The new method, although less accurate locally, improved the overall, or global, accuracy of the solution. The global accuracy is estimated by integrating the mass flux across the shock layer and comparing it with the known flux in the freestream. Further, it was found that the global error correlates with the mesh Damköhler number [Eq. (26)]. This is illustrated in Fig. 5.

In regard to the loss of accuracy at large mesh Damköhler numbers, it is worth noting that the use of conservation law variables does not seem to help as it does with ordinary gasdynamic shocks. The reason is that, for example, $(\rho u q_i)$ is continuous across a gasdynamic shock, but is discontinuous across a chemical reaction front.

Cones at Zero Incidence

We now consider the flow over pointed and spherically blunted cones with a 30 deg half-angle. The sphere radius of the blunted cone is 1.11 m. The freestream velocity is 6.7 km/s and freestream conditions correspond to 65.5 km altitude. These conditions are typical of a Space Shuttle trajectory point, and the 30 deg cone angle produces a shock strength about the same as for the Shuttle windward-side shock.

Figure 6 gives the distribution of atomic oxygen between the body and shock at various axial positions. The blunt-cone result is depicted by the solid line and the pointed cone by the dashed line. Note that the two results agree near the shock but differ greatly in the entropy layer near the body (compare Figs. 2 and 3). At an axial distance of about three nose radii, the blunt-nose solution has developed a severe undershoot in the atomic oxygen relative to the pointed cone profile. This is typical of blunt-nose entropy layers.

For wedge flow, a chemical reaction front limited the calculation of these flight conditions; however, for a blunt nose, the entropy layer develops more rapidly than the chemical reaction discontinuity near the bow shock wave. An oscillatory solution developed near the body when the blunt-nose case was computed much past $x/Rn = 15$. The oscillations are analogous to those obtained with the Lax-Wendroff type of finite difference scheme applied to

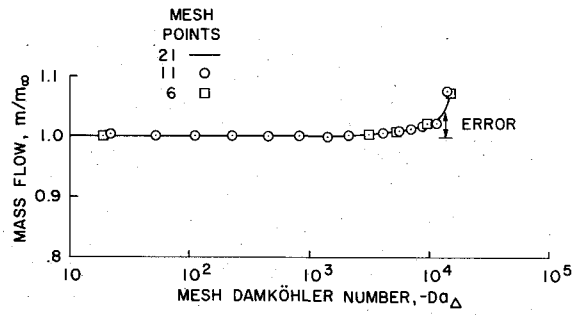

Fig. 5 Correlation of mass flow error with mesh Damköhler number.

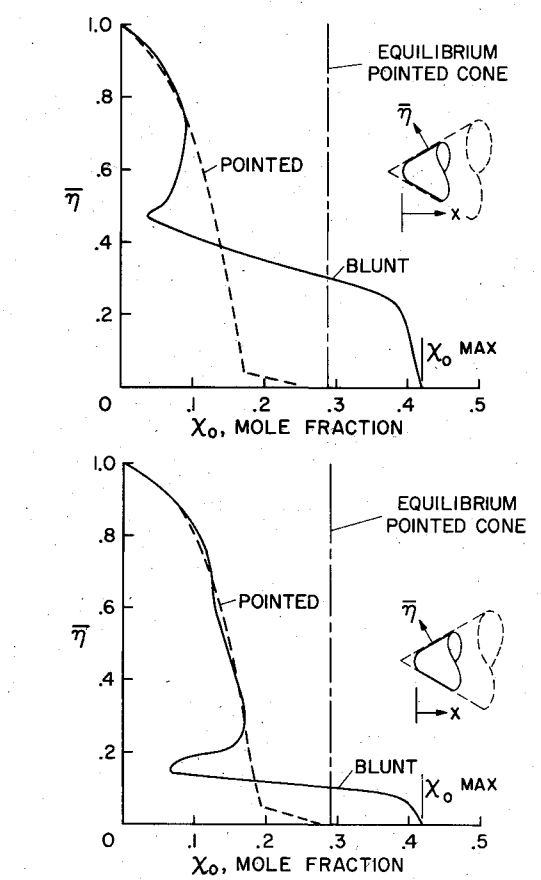

Fig. 6 Atomic oxygen profile for nonequilibrium flow over cones, $\theta_c = 30$ deg, $R_N = 1.11$ m, $V_\infty = 6.7$ km/s, altitude = 65.5 km: a) $x/R_N = 3$; b) $x/R_N = 6.8$.

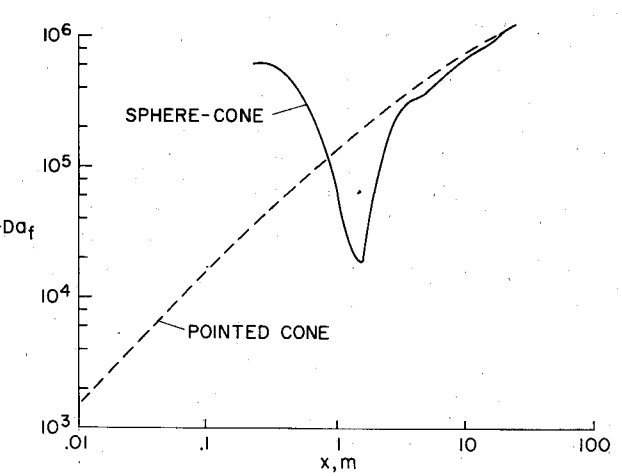

Fig. 7 Damköhler number for cones, $\theta_c = 30$ deg, $R_N = 1.11$ m, $V_\infty = 6.7$ km/s, altitude = 65.5 km.

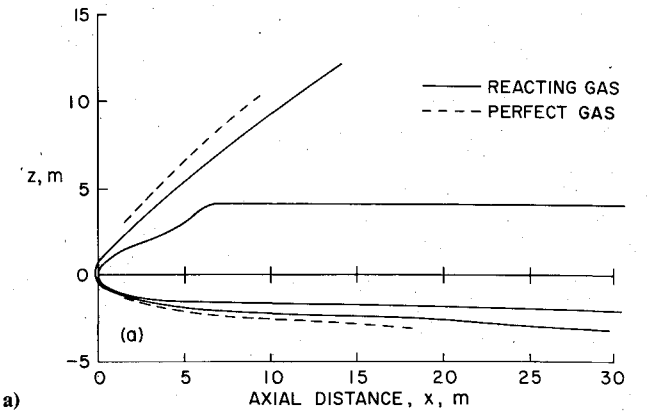

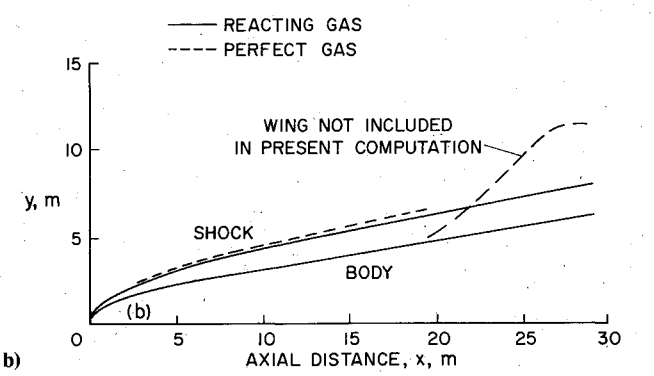

Fig. 8 Shock shape for Shuttle 147 body, $\alpha = 30$ deg, $V_\infty = 6.7$ km/s, altitude = 65.5 km: a) side view; b) plan view.

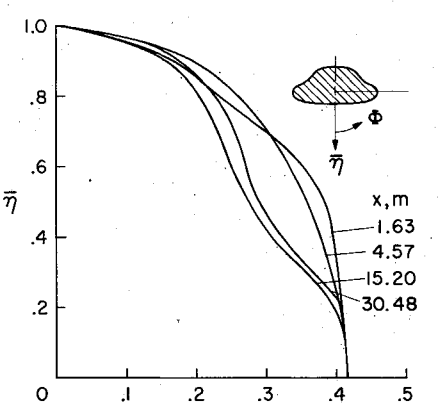

Fig. 9 Atomic oxygen profile on $\Phi = 0$ for Shuttle 147 body, $\alpha = 30$ deg, $V_\infty = 6.7$ km/s, altitude = 65.5 km.

discontinuous flows. Numerical smoothing can be used to eliminate the oscillations.[17]

The Damköhler number based on ψ [Eq. (25)] is shown in Fig. 7. Note that Da is evaluated using (ρV) behind the bow shock wave. For a blunted nose, the Damköhler number peaks near the sphere-cone juncture and then undershoots the pointed-cone result. Based on the previously shown oxygen profiles, it is concluded that the present flow is appreciably out of equilibrium for $10^3 < Da < 10^6$. For $Da \ll 10^3$ the flow is nearly frozen, and for $Da \gg 10^6$ the flow approaches equilibrium

Space Shuttle Orbiter

An important part of the Space Shuttle design effort involves computer predictions of the nonequilibrium flight envelope for the reusable orbiter vehicle. As a final example, therefore, some flow parameters are presented for the orbiter body shape at 30 deg angle of attack. The freestream conditions are for an altitude of 65.5 km (see Table 6). For these

Shuttle results, a single value, $\gamma_1 = \gamma_2 = 4/3$, was used for the specific heat ratio [see Eq. (23)], in order to match the conditions of the blunt-body starting solution.

To provide some feel for the effects of nonequilibrium chemistry, the Shuttle results are compared with perfect-gas (frozen) computations at the same freestream Mach number. In Fig. 8 the bow shock shapes are shown for the side and plan views. The shock standoff distance is decreased by the chemical reactions, as is expected.

Figure 9 shows the radial distribution of atomic oxygen at several stations and on the windward plane of symmetry. The same general trends noted previously for a blunt cone are seen to develop here also. At a distance of 15.2 m the oxygen distribution shows a thin reaction zone near the shock, a developing entropy layer near the body, and a somewhat constant region in between.

Conclusions

A computer code based on the method of characteristics has been used to perform an exploratory study of nonequilibrium flow over sharp- and blunt-nosed bodies. Because the structure of these nonequilibrium flows is too complex for analytical treatment and is difficult to obtain experimentally, one must rely on computational methods to provide knowledge of the flow. However, the lack of experimental data also makes it difficult to verify the correctness of the computer code. For these reasons it is informative to study the flow over simple shapes (i.e., sharp wedges) and pointed and blunted cones where at least the limiting solutions are exact.

By computing some flows over simple shapes, it was found that the numerical solution was strongly influenced by a nondimensional parameter, the mesh Damköhler number, which is a measure of the ratio of flow to reaction times. Reasonable accuracy can be maintained for a mesh Damköhler number less than about 10^4. At larger values, problems occur in the computation near the shock wave that prevent the computation of near-equilibrium flows. This computational difficulty is a direct consequence of a physical phenomenon, termed a chemical reaction front, that occurs in near-equilibrium flows.

On the basis of the present results, it is suggested that a Damköhler number based on the axial distance from the nose can be used to estimate the degree of nonequilibrium. For $Da_x > 10^6$, the flow is found to be near equilibrium, and for $Da_x < 10^3$ the flow is essentially frozen. The Damköhler number should be useful as a similarity parameter to extend to other flight conditions the sample results presented herein for the Space Shuttle orbiter body.

References

[1] Rakich, J. V., Stewart, D. A., and Lanfranco, M. J., "Results of a Flight Experiment on the Catalytic Efficiency of the Space Shuttle Heat Shield," AIAA Paper 82-0944, June 1982.

[2] Treanor, C. E., "A Method for the Numerical Integration of Coupled First-Order Differential Equations with Greatly Different Time Constant," *Mathematics of Computation,* Vol. 2, No. 93, Jan. 1966, pp. 39-45.

[3] Lomax, H. and Bailey, H. E., "A Critical Analysis of Various Numerical Integration Methods for Computing the Flow of a Gas in Chemical Nonequilibrium," NASA TN D-4109, 1967.

[4] Bailey, H. E., "A Numerical Integration of the Equations Governing the One-Dimensional Flow of a Chemically Reactive Gas," *Physics of Fluids,* Vol. 12, Nov. 1969, pp. 2292-2300.

[5] Der, J. J., "Theoretical Studies of Supersonic Two-Dimensional and Axisymmetric Nonequilibrium Flow, Including Calculations of Flow Through a Nozzle," NASA TR R-164, 1963.

[6] Marrone, P. V., "Inviscid Nonequilibrium Flow About Blunt Bodies and Normal Shock Waves, Part 1: General Analysis and Numerical Examples," Cornell Aeronautical Laboratory, Inc., Cal Rept. QM-1626-A-121, 1963.

[7] South, J. C., "Application of the Method of Integral Relations to Supersonic Nonequilibrium Flow Past Wedges and Cones," NASA TR R-205, Aug. 1964.

[8] Spurk, J. H., Gerber, N., and Sedney, R., "Characteristic Calculation of Flowfields With Chemical Reactions," *AIAA Journal,* Vol. 4, Jan. 1966, pp. 30-37.

[9] DeJarnette, F. R., "Two Different Interpretations of Measured Dissociation-Rate Constants and Their Effects on Coupled Vibrational-Dissociational Flows of Oxygen over a Wedge," NASA TN D-4028, July 1967.

[10] Kyriss, C., "A Time Dependent Solution for the Blunt Body Flow of a Chemically Reacting Gas Mixture," AIAA Paper 70-771, 1970.

[11] Taylor, A. A. and Hoffman, J. D., "Design of Maximum Thrust Nozzles with Nonequilibrium, Chemically Reacting Flow," AFAPL-TR-71-92,1, 1971.

[12] Li, C. P., "Time-Dependent Solutions of Nonequilibrium Dissociating Gases Past a Blunt Body," *Journal of Spacecraft and Rockets,* Vol. 9, Aug. 1972, pp. 571-572.

[13] Rakich, J. V. and Park, C., "Nonequilibrium Three-Dimensional Supersonic Flow Computations with Application to the Space Shuttle Orbiter Design," paper presented at the Symposium on Application of Computers to Fluid Dynamic Analysis and Design, Polytechnic Institute of Brooklyn Graduate Center, Farmingdale, New York, Jan. 1973.

[14] Rizzi, A. and Bailey, H., "Reacting Nonequilibrium Flow Around the Space Shuttle Using a Time Split Method," paper presented at the NASA Conference of Aerodynamic Analyses Requiring Advanced Computers, March 1974.

[15] Vincenti, W. G. and Kruger, C. H., *Introduction to Physical Gas Dynamics,* John Wiley & Sons, New York, 1965.

[16] Rakich, J. V. and Cleary, J. W., "Theoretical and Experimental Study of Supersonic Steady Flow Around Inclined Bodies of Revolution," *AIAA Journal,* Vol. 8, March 1970, pp. 511-518.

[17] Rakich, J. V., "A Method of Characteristics for Steady Three-Dimensional Supersonic Flow with Application to Inclinded Bodies of Revolution," NASA TN D-5341, 1969.

[18] Lighthill, M. L., "Dynamics of Dissociating Gas, Part I: Equilibrium Flow," *Journal of Fluid Mechanics,* Vol. 2, Pt. 1, 1957, pp. 1-32.

[19] Hilsenrath, J. and Klein, M., "Tables of Thermodynamic Properties of Air in Chemical Equilibrium Including Second Virial Corrections from 1500° K to 15,000° K," Arnold Engineering Development Center, Rept. TDR-63-161, 1964.

[20] Logan, J. G. and Treanor, C. E., "Tables of Thermodynamic Properties of Air from 3000° K to 10,000° K at Intervals of 100° K," Cornell Aeronautics Lab. Rept. BE-1007-A-3, 1957.

[21] Crowley, W. P., "Numerical Advection Experiments," *Monthly Weather Review,* Vol. 96, Jan. 1968, pp. 1-11.

[22] MacCormack, R. W., "The Effect of Viscosity in Hypervelocity Impact Cratering," AIAA Paper 69-354, Jan. 1969.